Atomic and electronic structures of N interstitials in GaAs

Eero Arola, Jussi Ojanen, Hannu-Pekka Komsa, and Tapio T. Rantala

Institute of Physics, Tampere University of Technology, P.O. Box 692, FIN-33101 Tampere, Finland

We have carried out electronic structure calculations on N interstitials in GaAs alloys using the first-principles plane-wave pseudopotential (PWPP) and projector augmented-wave (PAW) electronic structure methods in the framework of the density functional theory (DFT). Both the ultrasoft pseudopotential (USPP) method in connection with the generalized gradient approximation (GGA) and the PAW method in connection with the local density approximation (LDA) have been employed. Effects of the single nitrogen atom and nitrogen dimer related interstitial defects on the atomic and electronic structures of GaAs have been studied. Total energies, electronic band structures, and local densities of states have been evaluated. In general, energies of the defects with the NN dimer at the center of the Ga or As tetrahedron are more than 2 eV lower per nitrogen atom than those with a single N impurity at the same sites. We have also found that there are metastable defect candidates with a single N impurity in the middle of a particular edge of the Ga or As tetrahedra. Considering the modifications of the atomic structure of GaAs, our calculations show that the relaxations of the nearest neighbor atoms around the NN dimer at the center of the Ga or As tetrahedron, are essentially smaller than those around the single N impurity at the center of an edge of the Ga tetrahedron. Finally, these defect states induce drastic modifications into the electronic structure of GaAs. Interestingly, the NN dimer related defects cause noticeable changes only to the conduction bands near the conduction band edge, while the single N impurity related defects mainly modify the valence band edge and also induce localized and delocalized states into the band gap. Notably, the NN dimer and N impurity related defects lead to redshift and blueshift behavior of the band gap, respectively. The blueshift behavior is tentatively supported by the recent photoluminescence experiments.

I. INTRODUCTION

Alloying of GaAs with nitrogen has proved to be a challenge for crystal growth techniques, due to the low efficiency of N incorporation combined with a severe miscibility gap in the alloy phase diagram. Therefore, it will be important to understand the nature and energetics of N impurities in GaAs as a starting point for the growth process. Also, this serves as preliminary stage for the studies of a GaInAsN quaternary compound, which is expected to have significance in future optoelectronics.

$Ga_{1-y}In_yAs_{1-x}N_x$ and $GaAs_{1-x}N_x$ have recently become important members of a new class of semiconductor alloys, where electronic structure properties can drastically change when the nitrogen concentration increases from ultradilute ($\leq 0.01\%$) to a few percent.[1,2]

Experimental interest in group-III nitrides, III-V-N alloys, and, in particular, $GaAs_{1-x}N_x$ alloys, has been burgeoning since the early 1990s,[3–6] while their theoretical studies have started slightly later.[7–9] The apparent lack of interest in the past in studies of $Ga_{1-y}In_yAs_{1-x}N_x$ and $GaAs_{1-x}N_x$ alloys may partly be attributed to the large miscibility gap existing in these materials, which therefore leads to phase separation when the N composition is appreciable.[6,10,11] In the absence of detailed information on the miscibility gap, it is believed that the amount of nitrogen that can be incorporated into the $GaAs_{1-x}N_x$ alloy is limited to a few percent.[12] The typical nitrogen composition values (x) in $GaAs_{1-x}N_x$ bulk-like samples (layer thickness $> 0.5\ \mu$m) are smaller than 0.03.[13,14]

However, suitably grown $GaAs_{1-x}N_x$ thin film samples (layer thickness $\leq 0.5\ \mu$m)[6,11–13,15] can incorporate substantially larger amounts of nitrogen, close to $x=0.20$ values, have been reported.[6,12] Bandić *et al.*[16] have studied the temperature dependence of the growth kinetics of $GaAs_{1-x}N_x/GaAs$ superlattices, and found that even $x \approx 0.30$ can be achieved. By using a first-principles pseudopotentials method in the framework of the density functional theory (DFT) with the local density approximation (LDA) and the Boltzmann statistics, Zhang and Wei were able to show that the solubility of nitrogen in epitaxially grown $GaAs_{1-x}N_x$ films could be enhanced by several orders of magnitude, as compared to the bulk case.[17]

Among the first experimental studies, done in order to understand nitrogen effects in GaAs, are the observations of excitonic recombination due to isolated nitrogen (N_x) by Wolford *et al.*[18] and due to nitrogen-pair complexes (NN_i) by Liu *et al.*[3,4] Since then experiments for $GaAs_{1-x}N_x$ alloys between an ultradilute and a concentrated regime have been carried out.

Bandgap behavior in $GaAs_{1-x}N_x$ alloys has been studied by using photoluminescence,[5,12] optical absorption,[11] and electroreflectance[14] spectroscopies. These measurements unanimously show a redshift behavior of the bandgap, i.e., a reduction of the bandgap energy, and a composition-dependent bowing parameter[11,12] for small values of x (a few percent). These observations are further supported by several theoretical studies.[8–10,19,20]

After the tentative suggestion by Weyers and Sato[5] that N atoms are incorporated into group-V sites, several recent ex-

periments confirm this by showing that most of the nitrogen atoms in $GaAs_{1-x}N_x$ alloys ($0 < x < 0.03$) occupy substitutionally As sites, while a small fraction of the nitrogen atoms build up interstitial defects of various types (single N, NN dimer, N-As complex, etc.).[22–24] Furthermore, the nuclear reaction analysis (NRA) measurements by Ahlgren *et al.*[23] reveal that the concentration of interstitial nitrogen stays nearly constant ($\sim 2 \times 10^{19}$ cm^{-3}), while the substitutional part of it increases linearly (from $\sim 2 \times 10^{20}$ cm^{-3} upward) over the whole studied concentration regime.

Interestingly, Loke *et al.*[25] have recently demonstrated that blueshift-redshift and redshift-blueshift variations of the photoluminescence (PL) peak energy can be introduced into $GaAs_{1-x}N_x$ thin films by applying rapid thermal annealing (RTA). They suggested that the blueshift (redshift) might be due to the diffusion of the substitutional nitrogen atoms into nearby interstitial sites (and *vice versa*). This proposition is supported by the recent NRA measurements,[23] which show a drastic change in the concentration of interstitial nitrogen under the RTA.

Theoretical studies of $GaAs_{1-x}N_x$ alloys or mixed III-N nitrides in the past have exploited first-principles electronic structure methods within the framework of the DFT with the LDA [plane-wave pseudopotential (PWPP) method,[7,10,17,19,20] projector augmented-wave (PAW) method,[21] relativistic linearized augmented plane wave method (RLAPW),[9] and linear muffin-tin orbital (LMTO) method in the atomic sphere approximation (ASA)[26]], empirical pseudopotential method (EPM) combined with the valence force field (VFF) method,[8,27–29] and the tight-binding (TB) method.[1]

All-electron LMTO-ASA and RLAPW linearized electronic structure methods have been applied to bandgap bowing and lattice constant calculations in $Ga_{1-x}In_xN$[26] and $GaAs_{1-x}N_x$ alloys,[9] respectively. However, tackling many other physical problems of nonconventional, isovalent alloys (e.g., $GaP_{1-x}N_x$ and $GaAs_{1-x}N_x$) requires computational tools that can handle large (~ 100 atoms per unit cell) or even enormously large ($\sim 10\,000$ atoms per unit cell) supercells. The state-of-the-art *ab initio* PWPP method with the LDA and maximum of 64 atoms per unit cell has been used for studying phase stability in $GaAs_{1-x}N_x$ alloys,[10] electronic structure and formation energies of nitrogen-related substitutional complexes in GaAs,[19] nitrogen solubility, and defect formation energies in epitaxially grown $GaAs_{1-x}N_x$ films,[17] and electronic structure, atomic geometry, and the formation energies of substitutional nitrogen in GaAs.[20] Problems requiring even larger sizes of the unit cell can be tackled through parametrized electronic structure methods. The TB method with a 216-atom supercell has been applied to study the bandgap structure of $Ga_{1-y}In_yAs_{1-x}N_x$ alloys due to the nearest-neighbor environment of N,[1] and the EPM-VFF method with supercells containing $\sim 500-10\,000$ atoms has been applied to localization and percolation in a $GaAs_{1-x}N_x$ versus conventional, isovalent $GaAs_{1-x}P_x$ alloy,[8] effects of atomic short-range order on electronic and optical properties,[27] localized-delocalized state transition,[28] and electronic structure evolution in $GaAs_{1-x}N_x$ and $GaP_{1-x}N_x$ alloys when x changes from the ultradilute regime ($x < 0.01\%$) to a few percent.[29]

In this paper, we present theoretical results on energetics of various *interstitial*-type nitrogen defects in the GaAs crystal and their effects on its electronic band structure and local densities of states. Previous theoretical studies on nitrogen-related defects and alloying effects in GaAs and $GaAs_{1-x}N_x$ alloys have assumed nitrogen atoms to be placed substitutionally onto the group-V sublattice.[17,19,20,27–29] However, Zhang and Wei[17] have theoretically studied N-N and N-As split interstitial-type defects in epitaxial GaAs:N films, and more recently Carrier *et al.*[21] have studied N-N split interstitials in $GaAs_{1-x}N_x$ alloys by using the PAW-LDA method.

Our main findings are briefly described in the following (for further details, see Sec. III).

(i) There are substantial total energy variations among the single- and double- (dimer) nitrogen interstitials in GaAs.

(ii) On the basis of energetic considerations of these interstitials, we find that the most probable interstitial defect candidates in GaAs are the following three: the NN dimer at the center of the Ga- or As-related tetrahedron, and the single N impurity in the middle of one edge of the Ga tetrahedron.

(iii) Both the Ga and As tetrahedron-related NN dimer interstitials induce very similar changes to the GaAs electronic structure, while the changes due to the single N impurity-type interstitials are qualitatively quite different from the NN dimer interstitial causing modifications.

(iv) Both of the NN dimer interstitials cause a small redshift to the bandgap by decreasing it some 30 meV. On the other hand, all studied single N impurity interstitials cause the bandgap to become larger, i.e. referring to a *blueshift* that is tentatively supported by the recent experiments of Loke *et al.*[25] Notably, the Ga tetrahedron-edge-related single N impurity interstitial increases the bandgap by a substantial amount of 200 meV. As the substitutional nitrogen in GaAs is known to cause a drastic redshift effect, it is obvious that the nitrogen-related interstitials and substitutionals in $GaAs_{1-x}N_x$ have very different kinds of effects on the bandgap behavior and optical properties.

II. METHODS

The calculations were carried out using the first-principles plane-wave pseudopotential (PWPP) electronic structure method in the framework of the density functional theory (DFT). Both CASTEP (Cambridge Sequential Total Energy Package)[30] and VASP (Vienna *ab initio* Simulation Package)[31] computational schemes have been employed. For the studies of N interstitials in GaAs, the CASTEP scheme has been used in connection with the ultrasoft pseudopotential (USPP) method[32] and the generalized gradient approximation (GGA), while the VASP scheme has been used in connection with the projector-augmented wave (PAW) method[33,34] and the LDA.

In order to check the consistency between the CASTEP and VASP results, we have applied these schemes for GaAs in connection with the USPP-GGA method. In general, both codes seem to give very similar results to the electronic structures of GaAs and GaAs with various nitrogen interstitials. However, the computed energy bandgap values from these two codes differ to some extent. For example, the

bandgap values of GaAs in the CASTEP and VASP calculations become 0.58 and 0.63 eV, respectively. On the other hand, the VASP scheme using the PAW-LDA method, gives a value of 0.51 eV for the bandgap. The differences between the bandgap values, computed using the CASTEP and VASP schemes within the USPP-GGA method can be attributed to differences in the ultrasoft potentials used and to differences in the implementations of the two schemes.[35]

For the N interstitials in GaAs studies, ultrasoft pseudo-potentials and PAW potentials were used, while all Ga $3d$ electrons were included as valence electrons. Therefore, we choose 13, 5, and 5 valence electrons for Ga, As, and N, respectively. The exchange-correlation potential is modeled within the GGA (PW91)[36] and LDA (CA-PZ)[37,38] approximations. All our calculations were performed using a cubic 64-atom supercell geometry consisting of $2 \times 2 \times 2$ 8-atom GaAs unit cells. The size and symmetry of the supercell were fixed to those computed for pure GaAs ($a = 2 \times 5.627$ Å). Consequently, in GaAsN calculations the positions of all the atoms inside the supercell were allowed to relax. All CASTEP and VASP calculations within the USPP-GGA method were performed using one **k** point (Γ) for the Brillouin zone sampling, while the VASP calculations within the PAW-LDA method were carried out using the Monkhorst-Pack $2 \times 2 \times 2$ scheme of **k** points. We also found that the plane wave cutoff energy of 400 eV is sufficient for our present studies.

Our test calculations also show that the inclusion of the finite basis set correction (FBSC)[39] into the CASTEP calculation does not essentially change the results. For all the defect cases studied, we placed two nitrogen atoms into particular high-symmetry interstitial positions of the GaAs supercell. Consequently, the nitrogen concentration is about 6%, as measured with respect to the As sublattice. However, from the symmetry and bonding viewpoint, it is plausible that the nitrogen interstitials belonging to different supercells interact with each other only weakly. Also, the supercell lattice constant is fixed to that of pure GaAs. Therefore, we could conclude that the local environment of N in our calculations corresponds to that of a dilute concentration.

It has been well recognized by now that the electronic properties of GaAsN disordered alloys may not be rigorously studied by using conventional electronic structure methods (e.g., methods based on some mean-field-type approach like the virtual crystal and coherent potential approximation, or methods based on modeling the alloy as a periodic crystal composed of small supercells), which ignore the random fluctuations present in the polymorphous alloys.[28,29] However, the first-principles state-of-the-art PWPP method within the framework of the DFT gives a highly accurate account of the electronic structure for our fictive case of an ordered GaAsN alloy.

III. RESULTS AND DISCUSSION

The following N interstitial configurations are studied: a single N impurity at the center of the Ga tetrahedra (I_N^{tGa} defect), single N impurity in the middle of one specific edge of the Ga tetrahedra (I_N^{eGa} defect), and a NN dimer at the center of one Ga tetrahedron (I_{NN}^{tGa} defect). Similarly, the As
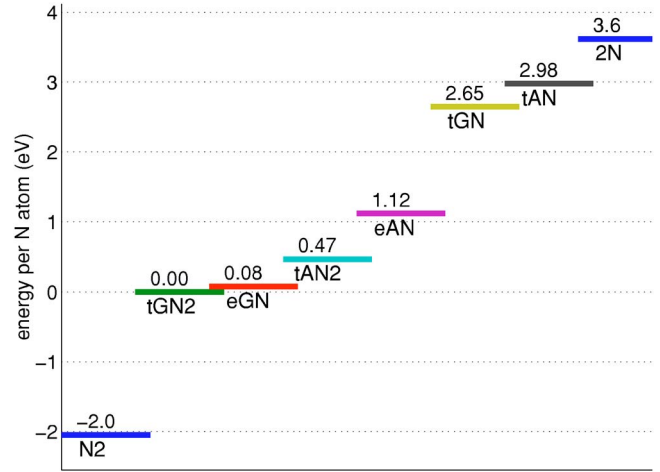

FIG. 1. (Color online) Energetics of various single N atom and NN dimer-related interstitial defects in GaAs, computed using the CASTEP (within the USPP-GGA method) scheme. Single N atom related defects are denoted by symbols eGN (I_N^{eGa}), eAN (I_N^{eAs}), tGN (I_N^{tGa}), and tAN (I_N^{tAs}), and the NN dimer-type defects by symbols tGN2 (I_{NN}^{tGa}) and tAN2 (I_{NN}^{tAs}) (for further details see the text). For comparison, we have also computed total energies for two extreme cases: one with pure GaAs crystal and a free N_2 molecule (N2), and the other one with a pure GaAs crystal and two separate N atoms outside of it (2N). The same stoichiometry has been used in all cases. The energy zero has been chosen as the total energy of the supercell (per N atom) with one I_{NN}^{tGa} type of an interstitial defect.

tetrahedra-related defects can be defined, namely, I_N^{tAs}-, I_N^{eAs}-, and I_{NN}^{tAs} defects. All these defects are located in the close vicinity of and around the [111] diagonal of the supercell. Although we have done theoretical studies on all the above-mentioned defect types in GaAs, we limit our discussion in this paper mostly to the three lowest-energy interstitials.

In all N interstitial cases studied, the computed GaAs structure serves as an initial atomic configuration of the supercell, before the geometry optimization (atomic relaxation), and the two nitrogen atoms have been placed into appropriate high-symmetry positions of the supercell. In particular, in the I_{NN}^{tGa} and I_{NN}^{tAs} interstitial cases, the center of mass (CM) of the NN dimer is initially at the CM of the Ga- and As-related tetrahedron,[40] respectively, and is directed along the [111] direction. In the I_N^{eGa} interstitial case, the first and the second N atom has been placed at the middle of the $[(1/2, 1/2, 1), (1, 1/2, 1/2)]$ edge of the Ga tetrahedron (1) and at the middle of the equivalent edge $[(3/2, 3/2, 2), (2, 3/2, 3/2)]$ of the Ga tetrahedron (2), respectively.[40]

In Fig. 1 the energetics of various types of interstitial defects (after atomic relaxation), as computed using the CASTEP scheme within the USPP-GGA method, is shown. All energies shown are the total electronic energies per nitrogen atom within the supercell with respect to the energy of the I_{NN}^{tGa} type of a defect. It clearly can be observed that the I_{NN}^{tGa}, I_N^{eGa}, and I_{NN}^{tAs} defect configurations from energetic viewpoints are the most probable ones, while the I_N^{eAs}, I_N^{tGa}, and I_N^{tAs} interstitial defects are located at much higher energies, and therefore these metastable states are not discussed here.

TABLE I. Total energies per nitrogen atom within the supercell (in eV) of various single N atom and NN dimer-related interstitial defects in GaAs, calculated using CASTEP and various VASP computational schemes. The same stoichiometry has been used in all cases. The energy zero has been chosen as the total energy of the supercell (per N atom) with one I_{NN}^{tGa} type of an interstitial defect.

	CASTEP[a]	VASP1[b]	VASP2[c]	VASP3[d]
I_{NN}^{tGa}	0	0	0	0
I_{N}^{eGa}	0.08	0.35	1.06	0.68
I_{NN}^{tAs}	0.47	0.53	0.43	0.33
I_{N}^{eAs}	1.12	1.18	1.87	1.45
I_{N}^{tGa}	2.65	2.59	2.92	2.28
I_{N}^{tAs}	2.98	3.14	3.27	2.59

[a]In connection with the USPP-GGA method.
[b]In connection with the USPP-GGA method and CASTEP (within the USPP-GGA method) optimized atomic structure.
[c]In connection with the PAW-LDA method and CASTEP (within the USPP-GGA method) optimized atomic structure.
[d]In connection with the PAW-LDA method that also optimizes the atomic structure.

It is important to notice that the total energy changes due to atomic relaxation from the initial to the minimum-energy optimized final atomic configuration vary quite substantially between the different interstitial cases. These total energy changes within the supercell (per nitrogen atom) for I_{NN}^{tGa}, I_{NN}^{tAs}, and I_{N}^{eGa} interstitial cases are −0.23, −0.37, and −3.9 eV, respectively. Remarkably, the energy drop in the N edge interstitial case (I_{N}^{eGa}) is very large, therefore reflecting large local relaxations around the N impurity atom (see Sec. III B).

In Table I the total energies of the above-mentioned interstitial defects are presented that have been calculated using CASTEP (within the USPP-GGA method) and various VASP (within the USPP-GGA and PAW-LDA methods) computational schemes.

It can be seen from Table I that CASTEP and VASP schemes lead qualitatively to a similar behavior of the total energies within the USPP-GGA method (see CASTEP versus VASP1 results). However, there are some 3%–12% quantitative differences between the CASTEP and VASP1 total energies in the I_{NN}^{tAs}, I_{N}^{eAs}, I_{N}^{tGa}, and I_{N}^{tAs} interstitial cases, and an especially large difference in the I_{N}^{eGa} interstitial case. These differences are most probably due to the different ultrasoft pseudopotentials used in these two computational schemes and differences in the implementations of these codes. It is also noticeable from the VASP1 and VASP2 results of Table I that switching from the USPP-GGA method to the PAW-LDA one, while keeping the underlying atomic structure the same, inverts the energetical order of two low-energy lying interstitials, namely, I_{N}^{eGa} and I_{NN}^{tAs}.[41] Furthermore, VASP2 and VASP3 results of Table I show that the total energies in various interstitial cases, computed within the PAW-LDA method, are rather sensitive to the underlying atomic structure used. Therefore, it is important to optimize the atomic and electronic structures of these interstitial defects in GaAs using consistently the same computational scheme.

In the following we discuss the modifications occurring in the atomic and electronic structures of the GaAs crystal
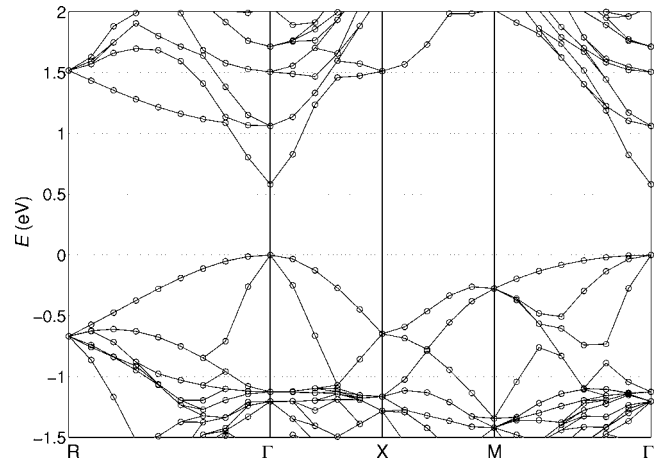
FIG. 2. Electronic band structure of a pure GaAs crystal along various high-symmetry directions of the Brillouin zone for the simple cubic (sc) $2 \times 2 \times 2$ supercell, computed using the CASTEP (within the USPP-GGA method) scheme. It has to be noticed that the solid line does not necessarily represent an irreducible representation of the group of **k** (along a symmetry direction) to which the band belongs. It rather serves as a guide to an eye. The valence-band maximum (VBM) has been chosen as the origin of the (relative) energy scale.

when various interstitial nitrogen-related defects are introduced into it. In Figs. 2, 3, 4, and 5 we show the electronic band structures of the supercell geometry for pure GaAs, and GaAs with I_{NN}^{tGa}-, I_{NN}^{tAs}-, and I_{N}^{eGa}-type defects, respectively, as calculated using the CASTEP scheme within the USPP-GGA method. In order to interpret these band structures nitrogen-, gallium-, and arsenic-derived local densities of states (LDOS) for the various defect cases are shown in Figs. 6, 7, and 8, respectively. The optimized electronic and atomic structures, and the resulting LDOS curves for these interstitial cases have been computed using the VASP scheme within the PAW-LDA method. In the LDOS formulation a one-center density matrix technique inside the PAW spheres has been exploited.[42]
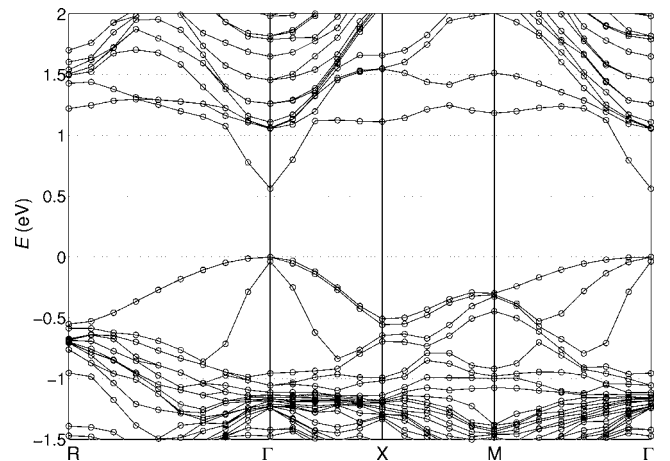
FIG. 3. The same as in the caption to Fig. 2, except that the I_{NN}^{tGa}-type interstitial defect has been placed into the GaAs supercell.
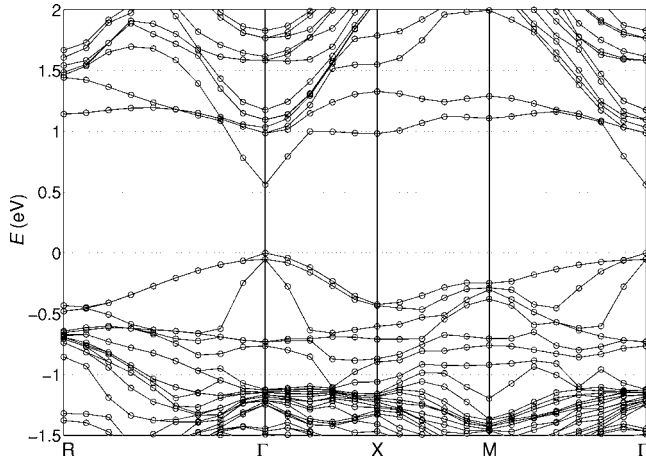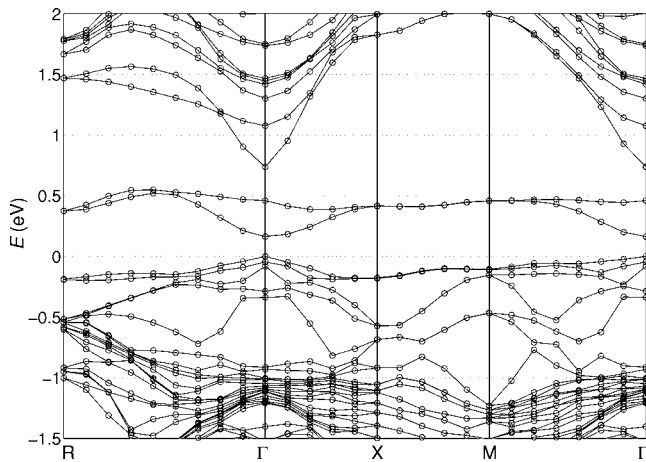
FIG. 4. The same as in the caption to Fig. 2, except that the $I_{\rm NN}^{t{\rm As}}$-type interstitial defect has been placed into the GaAs supercell.

A. NN dimer interstitials $I_{\rm NN}^{t{\rm Ga}}$ and $I_{\rm NN}^{t{\rm As}}$

We briefly discuss the modifications occurring in the atomic structure of GaAs when $I_{\rm NN}^{t{\rm Ga}}$- and $I_{\rm NN}^{t{\rm As}}$-type nitrogen dimer interstitials are placed in it.

Our calculations show that in both defect cases the total energy will be minimized when the nitrogen dimer is located on the main diagonal of the supercell[43] and oriented along its direction ([111]). Furthermore, the equilibrium positions of the nitrogen dimers in the $I_{\rm NN}^{t{\rm Ga}}$ and $I_{\rm NN}^{t{\rm As}}$ defect cases are such that their centers of mass are very close to the centers of mass of the Ga- and As-related tetrahedra, respectively.[44] We also notice that in $I_{\rm NN}^{t{\rm Ga}}$ and $I_{\rm NN}^{t{\rm As}}$ interstitial defect cases the bond length of the nitrogen dimer has been increased to the values of 1.15 and 1.13 Å, respectively, from the bond length for a free N_2 molecule (1.10 Å).

Considering the relaxation of Ga and As atoms, our calculations show that in the both interstitial cases the nearest atoms to the NN dimer (these are the vertices of the tetrahedron inside which the dimer is located) will experience substantial relaxation. In the $I_{\rm NN}^{t{\rm Ga}}$ ($I_{\rm NN}^{t{\rm As}}$) interstitial case, the Ga

FIG. 6. Nitrogen- (N-) derived local densities of states (LDOS) for different interstitials in GaAs: $I_{\rm NN}^{t{\rm Ga}}$ (dashed line), $I_{\rm NN}^{t{\rm As}}$ (dotted line), and $I_{\rm N}^{e{\rm Ga}}$ (dash-dotted line), computed using the VASP (within the PAW-LDA method) scheme. The horizontal lines indicate the position of the bandgap for GaAs (solid line) and various interstitial cases (line types as for the LDOS curves). Note that an absolute energy scale has been used in order to display the possible shift of the valence and conduction band edges.

(As) atoms at the top and base vertices of the Ga- (As-) related tetrahedron will experience 0.08 Å (0.29 Å) and 0.15 Å (0.21 Å) relaxations, respectively. On the other hand, the next nearest atoms become relaxed essentially to a smaller amount, and the more distant atoms experience hardly any relaxation. Incorporating the NN dimer inside an empty Ga- or As-related tetrahedron of the GaAs crystal causes the tetrahedron to be expanded symmetrically around the [111] main diagonal. The base edges of the tetrahedron in $I_{\rm NN}^{t{\rm Ga}}$ and $I_{\rm NN}^{t{\rm As}}$ interstitial cases will become increased by 6.4% and 8.8%, respectively. However, the side edges of the Ga- and As-related tetrahedra will experience quite different increases, being 4.4% and 10%, respectively.

FIG. 5. The same as in the caption to Fig. 2, except that two $I_{\rm N}^{e}$-type interstitial defects have been placed into the GaAs supercell.
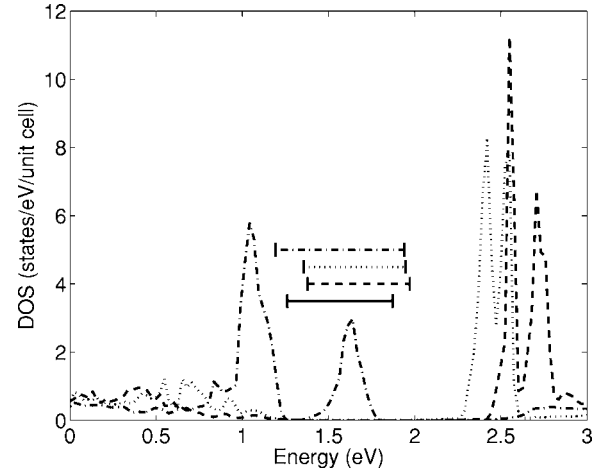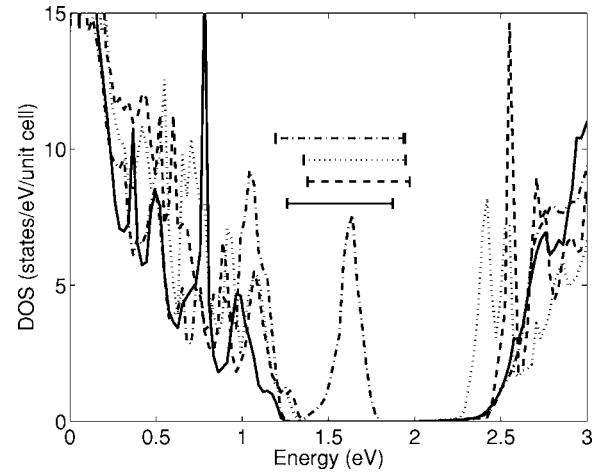

FIG. 7. Gallium- (Ga-) derived local densities of states for GaAs (solid line) and for different interstitials in GaAs: $I_{\rm NN}^{t{\rm Ga}}$ (dashed line), $I_{\rm NN}^{t{\rm As}}$ (dotted line), and $I_{\rm N}^{e{\rm Ga}}$ (dash-dotted line). For other details, see the caption to Fig. 6.
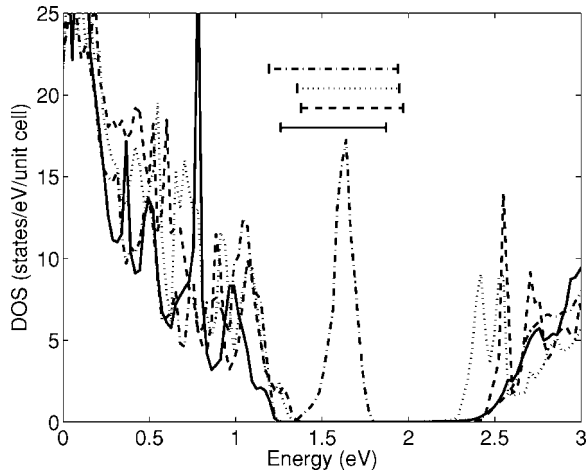
FIG. 8. The same as in the caption to Fig. 7, except for the arsenic- (As-) derived local densities of states.

We now turn to discuss the electronic structures. Interestingly, it can be observed that the I_{NN}^{tGa}- and I_{NN}^{tAs}-type defects cause very similar effects onto the GaAs electronic structure. First of all, it can be seen from Figs. 2–4 that the energy bandgap hardly changes from the calculated GaAs value, the change being of the order of 30 meV toward smaller energies, i.e., referring to a tiny redshift in the emission spectra, in both defect cases. On the other hand, experiments[5,11,12,14] and calculations[8,9,19,29] on GaAs$_{1-x}$N$_x$ indicate a rapid decrease of E_g for $x < \sim 0.02$, and a less rapid decrease for larger values of x.[11] From the optical absorption measurements of Ref. 11 we can see that the bandgap at $x=0.06$ has already decreased by amount of some 300 meV from that of GaAs (1.42 eV).

We have recently started *ab initio* electronic structure studies in the case of nitrogen substitutional-type defects in GaAs, by employing the PAW method with the LDA.[45] The calculations show that in the N$_{As}$ substitutional case (two N atoms with their minimum-energy configuration being along the [111] direction, replace two As atoms inside the supercell) the bandgap decreases by some 400 meV from the bandgap of GaAs. These values are fairly close to the experimentally observed value of 300 meV for the bandgap reduction.[11] Therefore, it looks as if the most preferable occupation site of nitrogen in GaAs$_{1-x}$N$_x$ alloy at around $x=0.06$ is substitutional, and the metastable interstitial I_{NN}^{tGa} and I_{NN}^{tAs} defects are less frequently present in that alloy. This is further substantiated by the recent experiments.[22–24]

Second, we notice from Figs. 3 and 4 that no impurity states or bands will form into the band gap in I_{NN}^{tGa}- and I_{NN}^{tAs} defect cases. This is obviously so, because the NN dimer inside either Ga- or As-related tetrahedra is highly stable and is not able to get hybridized with the surrounding atoms strongly enough to form new states into the gap.

Third, Figs. 3 and 4 for the electronic band structures of the I_{NN}^{tGa} and I_{NN}^{tAs} defect cases, respectively, together with Figs. 6, 7, and 8 for N, Ga, and As local densities of states, respectively, clearly indicate large modifications in the electronic structure near the *conduction band* minimum (CBM). In particular, the two narrow double-peak structures about 0.5 eV

above the CBM in Figs. 6–8 show that the nitrogen states experience a fairly strong localization there and at the same time hybridize with the host Ga and As states. Using the terminology of Kent and Zunger,[28,29] we could say that these states represent the perturbed host states (PHS) forming resonancelike (or virtual bound states) within the conduction band continuum. The localization and the double-peak structure in the Ga, As, and N local densities of states is further substantiated by the appearance of two rather disperseless bands around 1 eV in the conduction band region.

In contrast to the conduction band edge states, the I_{NN}^{tGa} and I_{NN}^{tAs} interstitials induce fairly small changes to the electronic structure near the *valence band* maximum (VBM). The Ga and As component densities of states (Figs. 7 and 8, respectively) clearly indicate that the Ga and As states within some 0.5 eV downward from the VBM move rather rigidly by ~ 100 meV toward higher energies while essentially retaining their localization nature when I_{NN}^{tGa}- and I_{NN}^{tAs} defects are incorporated into GaAs. However, Figs. 7 and 8 along with the band structures of Figs. 2–4 show that new, essentially disperseless PHS-like bands appear through Ga ($3p, 3d$) and As ($4p$) states localization between -1 and -0.5 eV with respect to the VBM.

B. Single N interstitial I_N^{eGa}

We briefly discuss the modifications occurring in the atomic structure of GaAs when a I_N^{eGa}-type single nitrogen atom interstitial is placed in it.

Our calculations show that the N edge interstitial that corresponds to the minimum-energy atomic configuration, after the atomic relaxation, is located at the distance of 0.6 Å from the center of a base edge of a Ga-related tetrahedron at $(3/4, 1/2, 3/4)$ [the edge is between the Ga atoms at $(1/2, 1/2, 1)$ and $(1, 1/2, 1/2)$].[40]

This N interstitial atom is very close to an As atom such that the As-N distance becomes 1.79 Å. During the relaxation, this As atom has been repelled away from the N atom by some 0.65 Å as compared to the position of the same As atom in GaAs at $(3/4, 1/4, 3/4)$. Therefore, we could consider this N interstitial defect to behave like an As-N dimer (see, for example, Fig. 3 of Ref. 17). Furthermore, the As atom of the As-N dimer is located at the center of mass of the Ga-related tetrahedron, whose top vertex point is at $(1,0,1)$, and the base vertex points at $(1, 1/2, 1/2)$, $(1/2, 1/2, 1)$, and $(1/2, 0, 1/2)$.[40]

We also notice that the nearest neighbor Ga atoms around the As and N atoms of the As-N split interstitial experience fairly large relaxations: 0.26 Å–0.27 Å and 0.36 Å, respectively. These relaxation values are essentially larger than the relaxations of the nearest neighbor atoms around the NN dimer in the I_{NN}^{tGa} and I_{NN}^{tAs} interstitial cases (see Sec. III A). As is the case with the I_{NN}^{tGa} and I_{NN}^{tAs} interstitials, the next nearest neighboring and more distant atoms experience only very minor relaxations in the N edge interstitial (As-N split interstitial) case.

We finally briefly discuss the modifications occurring in the electronic structure in GaAs due to I_N^{eGa}-type interstitial defects. From the computed electronic band structure (Fig. 5)

and the N, Ga, and As local densities of states (Figs. 6, 7, and 8, respectively) we immediately observe that the I_N^{eGa}-type defects cause qualitatively and quantitatively very different kinds of modifications to the electronic structure as compared to changes introduced by the I_{NN}^{tGa}- and I_{NN}^{tAs}-type defects.[47]

First, we observe an important phenomenon that the bandgap of the GaAs crystal with I_N^{eGa}-type defects incorporated in it has *increased* by some 200 meV as compared to that of the GaAs crystal, i.e., referring to the case of *blueshift*. This can be attributed to the appearance of nitrogen-derived impurity band states (see the discussion later) in the middle of the bandgap that causes a repulsion such that the conduction band edge moves toward higher energies.

To our knowledge, there is no experimental or theoretical evidence of the blueshift behavior while the concentration increases in GaAs$_{1-x}$N$_x$ alloys with x around 6% available.[46] However, on the basis of our calculations, we could tentatively propose that if the number of I_N^{eGa}-type defects in the GaAs$_{1-x}$N$_x$ samples could be increased (for example, by some appropriate annealing technique), then the blueshift should be experimentally observable. Interestingly, Loke *et al.*[25] have observed both blue- and redshift behavior in the photoluminescence (PL) spectra measured from GaAs$_{1-x}$N$_x$ films grown on GaAs (100) substrates for $x=1.3\%$ and 2.2%, the amounts of the blue- and redshift variations depending on the annealing conditions. According to their explanation, the blue- and redshift could have been caused by hopping of nitrogen atoms from substitutional (As) sites to nearby interstitial sites, and *vice versa*, respectively. Although we have not strictly confirmed this by our present calculations, this might be the case. However, our calculations do predict that there will be a blueshift in the PL spectra when interstitial defects of the I_N^{eGa} type are formed into the GaAs crystal.[48]

Second, our calculation reveals that two occupied bands with a relatively small overall dispersion over the whole Brillouin zone appears in the bandgap (see Fig. 5). From the existence of a strong peak within the gap region of the N, Ga, and As local densities of states, we can deduce that these bands derive from a hybridization between the N, Ga, and As electronic states, rather than the N-N interaction between nitrogen atoms of different unit cells. Consequently, these bands could be characterized as PHS-like bands instead of impurity bands. Our partial wave analysis (not shown here) reveals that some Ga $(3p, 3d)$ and As $(4p)$ states have moved up and hybridized with a large weight of N $(2p)$ states when forming the band states into the gap. Also, the dispersion behavior of these bands clearly indicates that the upper (deep level) band is composed of more localized states, while the lower band in the vicinity of the Γ point gains more delocalized character. This delocalization is in agreement with the tail behavior of the lower-energy side of the peak in the local densities of states within the bandgap (Figs. 6–8).

Finally, we discuss the electronic structure changes within the conduction and valence band continua of GaAs due to the I_N^{eGa}-type interstitials, and compare and contrast them to the changes due to the NN dimer (I_{NN}^{tGa} and I_{NN}^{tAs}) interstitials. From the calculated electronic band structures we can see that the modifications in the conduction and valence band continua caused by the I_N^{eGa}-type defects (Fig. 5) are qualita-

tively quite different from those caused by the I_{NN}^{tGa}- and I_{NN}^{tAs}-type interstitial defects (Figs. 3 and 4, respectively). For example, the *conduction band continuum* experiences far less dramatic changes when the I_N^{eGa} type of interstitial defects are placed into GaAs than in the case of I_{NN}^{tGa}- or I_{NN}^{tAs}-type defects. This is further supported by the fact that the Ga and As component densities of states in the conduction band continuum between the I_N^{eGa} interstitial case and GaAs are very similar (see Figs. 7 and 8). In particular, the conduction bands in the I_N^{eGa} defect case are highly delocalized throughout the BZ, while in the I_{NN}^{tGa} and I_{NN}^{tAs} defect cases localized bands appear in the conduction band continuum (see Sec. III A). This behavior is obviously due to the hybridization properties between the valence orbitals of a nitrogen atom (N) or nitrogen-dimer (NN) and the orbitals of the host gallium (Ga) and arsenic (As) atoms. Namely, in contrast to the I_{NN}^{tGa} and I_{NN}^{tAs} interstitial cases (see the discussion in Sec. III A), it can be seen from Fig. 6 that in the I_N^{eGa} interstitial case there are hardly any nitrogen states within ~ 1 eV above the CBM available, which could become hybridized with the host atom states.

On the other hand, by comparing Figs. 2–5 we can notice that the situation is quite the opposite when modifications in the *valence band continuum* are considered. Namely, the I_N^{eGa}-type defects cause a lot more drastic changes in the GaAs electronic structure than the I_{NN}^{tGa} and I_{NN}^{tAs} defects do within the range of 0.5 eV downward from the top of the valence band. It is now the localized N $(2p)$ states in the I_N^{eGa} defect case, just below the VBM, which become hybridized with the Ga $(3p, 3d)$ and As $(4p)$ states (see Figs. 6–8), leading to the highly disperseless bands just below the VBM (see Fig. 5). On the other hand, as already mentioned in Sec. III A, the dimer-type defects (I_{NN}^{tGa} and I_{NN}^{tAs}) only weakly perturb the host GaAs states within the same energy range (Figs. 3 and 4). For energies between -1 and -0.5 eV below the VBM, the single impurity defects I_N^{eGa} lead to only slightly perturbed host states (PHS) that retain the delocalized nature of the host bands. As Figs. 7 and 8 indicate, the Ga and As local densities of states suffer virtually no changes at all within this energy regime when the I_N^{eGa} defects are incorporated into GaAs. In contrast to this, the dimer defects I_{NN}^{tGa} and I_{NN}^{tAs} build up localized bands within the same energy regime, as already discussed in Sec. III A.

IV. CONCLUSIONS

We have studied the effects of the single nitrogen atom and nitrogen dimer-related interstitial defects on the atomic and electronic structures of GaAs within the framework of the density functional theory (DFT). From the energetical viewpoint, among several metastable interstitial defects studied, there are three of those whose related total energies are very close to each other. These are the dimer defects I_{NN}^{tGa} and I_{NN}^{tAs}, and the single impurity defect I_N^{eGa}.

Considering the modifications occurring in the atomic structure of GaAs, our calculations show that relaxations of the nearest neighbor atoms around the NN dimer in the I_{NN}^{tGa} and I_{NN}^{tAs} interstitial cases are essentially smaller than those around the As-N split interstitial in the I_N^{eGa} defect case. In all

these defect cases, the next nearest neighboring and more distant atoms experience only very minor relaxations.

Interestingly, the I_{NN}^{tGa}- and I_{NN}^{tAs}-type defects cause very similar changes to the electronic structure of GaAs, while I_N^{eGa}-type defects introduce qualitatively quite different kinds of modifications to the electronic structure. For example, the I_{NN}^{tGa}- and I_{NN}^{tAs}-type defects cause a small redshift related change of some 30 meV in the bandgap of GaAs, while I_N^{eGa}-type defects cause a *blueshift*-related change of about 200 meV.

On the other hand, it is well known from the experiments[5,11,12,14] and previous calculations[8,9,19,29] that the *substitutional* nitrogen-related defects in GaAs cause a drastic redshift effect, accompanied by a large composition-dependent bowing parameter at low values of x. In particular, at $x \approx 6\%$, our preliminary PAW-LDA calculations on GaAs$_{1-x}$N$_x$ alloys[45] indicate that the nitrogen substitutional defects N_{As} *reduce* the bandgap by about 400 meV, which is close to the experimentally observed value of 300 meV.[11] Furthermore, we have not found any experimental or theoretical evidence of a blueshift behavior-while increasing the concentration of nitrogen substitutionals at hypothetical x values smaller than 0.5.[46]

On the basis of that previous, we can see that the nitrogen-related interstitial- and substitutional-type defects in GaAs$_{1-x}$N$_x$ have qualitatively and quantitatively very different kinds of effects on the bandgap behavior and optical properties. This has recently been substantiated experimentally by Loke *et al.*,[25] who have found that the redshift behavior can be changed to the blueshift one, and *vice versa*, by a proper treatment of the GaAs$_{1-x}$N$_x$ samples. Hopefully, the present work will stimulate further experimental and theoretical studies on the effects of the interstitial defects in GaAs$_{1-x}$N$_x$ alloys.[48]

ACKNOWLEDGMENTS

[1] P. J. Klar, H. Grüning, J. Koch, S. Schäfer, K. Volz, W. Stolz, W. Heimbrodt, A. M. Kamal Saadi, A. Lindsay, and E. P. O'Reilly, Phys. Rev. B **64**, 121203(R) (2001).

[2] K. Kim and A. Zunger, Phys. Rev. Lett. **86**, 2609 (2001).

[3] X. Liu, M.-E. Pistol, L. Samuelson, S. Schwetlick, and W. Seifert, Appl. Phys. Lett. **56**, 1451 (1990).

[4] X. Liu, M.-E. Pistol, and L. Samuelson, Phys. Rev. B **42**, 7504 (1990).

[5] M. Weyers and M. Sato, Appl. Phys. Lett. **62**, 1396 (1993).

[6] C. T. Foxon, T. S. Cheng, S. V. Novikov, D. E. Lacklison, L. C. Jenkins, D. Johnston, J. W. Orton, S. E. Hooper, N. Baba-Ali, T. L. Tansley, and V. V. Tret'yakov, J. Cryst. Growth **150**, 892 (1995).

[7] A. F. Wright and J. S. Nelson, Appl. Phys. Lett. **66**, 3051 (1995).

[8] L. Bellaiche, S.-H. Wei, and A. Zunger, Phys. Rev. B **54**, 17568 (1996).

[9] S.-H. Wei and A. Zunger, Phys. Rev. Lett. **76**, 664 (1996).

[10] J. Neugebauer and C. G. Van de Walle, Phys. Rev. B **51**, 10568 (1995).

[11] W. G. Bi and C. W. Tu, Appl. Phys. Lett. **70**, 1608 (1997).

[12] J. Salzman and H. Temkin, Mater. Sci. Eng., B **50**, 148 (1997).

[13] R. S. Goldman, R. M. Feenstra, B. G. Briner, M. L. O'Steen, and R. J. Hauenstein, Appl. Phys. Lett. **69**, 3698 (1996).

[14] J. D. Perkins, A. Mascarenhas, Y. Zhang, J. F. Geisz, D. J. Friedman, J. M. Olson, and S. R. Kurtz, Phys. Rev. Lett. **82**, 3312 (1999).

[15] T. D. Veal, I. Mahboob, L. F. J. Piper, C. F. McConville, and M. Hopkinson, J. Appl. Phys. **95**, 8466 (2004).

[16] Z. Z. Bandić, R. J. Hauenstein, M. L. O'Steen, and T. C. McGill, Appl. Phys. Lett. **68**, 1510 (1996).

[17] S. B. Zhang and S.-H. Wei, Phys. Rev. Lett. **86**, 1789 (2001).

[18] D. J. Wolford, J. A. Bradley, K. Fry, and J. Thompson, in *Proceedings of the 17th International Conference on the Physics of Semiconductors*, edited by J. D. Chadi and W. A. Harrison (Springer-Verlag, New York, 1984), p. 627.

[19] J. E. Lowther, S. K. Estreicher, and H. Temkin, Appl. Phys. Lett. **79**, 200 (2001).

[20] W. Orellana and A. C. Ferraz, Appl. Phys. Lett. **78**, 1231 (2001).

[21] P. Carrier, S.-H. Wei, S. B. Zhang, and S. Kurtz, Phys. Rev. B **71**, 165212 (2005).

[22] W. Li, M. Pessa, and J. Likonen, Appl. Phys. Lett. **78**, 2864 (2001).

[23] T. Ahlgren, E. Vainonen-Ahlgren, J. Likonen, W. Li, and M. Pessa, Appl. Phys. Lett. **80**, 2314 (2002).

[24] W. J. Fan, S. F. Yoon, T. K. Ng, S. Z. Wang, W. K. Loke, R. Liu, and A. Wee, Appl. Phys. Lett. **80**, 4136 (2002).

[25] W. K. Loke, S. F. Yoon, S. Z. Wang, T. K. Ng, and W. J. Fan, J. Appl. Phys. **91**, 4900 (2002).

[26] W. R. L. Lambrecht, Solid-State Electron. **41**, 195 (1997).

[27] L. Bellaiche and A. Zunger, Phys. Rev. B **57**, 4425 (1998).

[28] P. R. C. Kent and A. Zunger, Phys. Rev. Lett. **86**, 2613 (2001).

[29] P. R. C. Kent and A. Zunger, Phys. Rev. B **64**, 115208 (2001).

[30] Accelrys Inc., CASTEP User's Guide, San Diego: Accelrys Inc., 2001. For further details behind the CASTEP code, see the review article: V. Milman, B. Winkler, J. A. White, C. J. Pickard, M. C. Payne, E. V. Akhmatskaya, and R. H. Nobes, Int. J. Quantum Chem. **77**, 895 (2000).

[31] G. Kresse and J. Furthmüller, Phys. Rev. B **54**, 11 169 (1996).

[32] D. Vanderbilt, Phys. Rev. B **41**, R7892 (1990).

[33] P. E. Blöchl, Phys. Rev. B **50**, 17953 (1994).

[34] G. Kresse and D. Joubert, Phys. Rev. B **59**, 1758 (1999).

[35] Our further test calculations on the VASP scheme reveal that when used in the connection with the PAW-GGA method for GaAs while allowing lattice relaxation, it gives a far too small bandgap

value of 130 meV. This bandgap behavior can be attributed to the lattice constant of 5.75 Å, which is essentially larger than the one computed using the VASP scheme within the PAW-LDA method (5.61 Å). Consequently, we have not used the VASP scheme within the PAW-GGA method in any of our present calculations.

[36] J. P. Perdew, J. A. Chevary, S. H. Vosko, K. A. Jackson, M. R. Pederson, D. J. Singh, and C. Fiolhais, Phys. Rev. B **46**, 6671 (1992).

[37] D. M. Ceperley and B. J. Alder, Phys. Rev. Lett. **45**, 566 (1980).

[38] J. P. Perdew and A. Zunger, Phys. Rev. B **23**, 5048 (1981).

[39] G. P. Francis and M. C. Payne, J. Phys.: Condens. Matter **2**, 4395 (1990).

[40] Our coordinate system is defined such that if we consider, for example, a GaAs crystal structure (zincblende), then a Ga atom sits at $(0,0,0)$ and its nearest As atom at $(1/4,1/4,1/4)$. Consequently, the vertex points of the Ga- and As-related tetrahedra used to define the various N interstitial defects, are described in the following. Ga tetrahedron (1): $(1,1,1)$ is the top vertex, and $(1/2,1/2,1)$, $(1/2,1,1/2)$, and $(1,1/2,1/2)$ are the base vertices; Ga tetrahedron (2): vertex points of Ga tetrahedron (1) $+(1,1,1)$; Ga tetrahedron (3): $(1,0,1)$ is the top vertex, and $(1,1/2,1/2)$, $(1/2,1/2,1)$, and $(1/2,0,1/2)$ are the base vertices; As tetrahedron (1): $(1/4,1/4,1/4)$ is the top vertex, and $(3/4,3/4,1/4)$, $(1/4,3/4,3/4)$, and $(3/4,1/4,3/4)$ are the base vertices. The Ga tetrahedron (1) and As tetrahedron (1) define the I_{NN}^{tGa} and I_{NN}^{tAs} interstitial defects, respectively, and Ga tetrahedra (1) and (3) are used when discussing the I_{N}^{eGa} interstitial defect.

[41] The methodological differences between the USPP-GGA and PAW-LDA methods of the VASP scheme obviously mostly contribute to the differences between the VASP1 and VASP2 results of Table I. However, a small contribution to these differences comes from the fact that the USPP-GGA calculations use one **k** point (Γ) for the Brillouin zone sampling, while the PAW-LDA calculations exploit the Monkhorst-Pack $2 \times 2 \times 2$ scheme of **k** points.

[42] G. Kresse (private communication, 2005).

[43] The main diagonal of the supercell is defined as the line along which the As sublattice with face-centered cubic (fcc) structure has to be displaced with respect to the Ga fcc sublattice, in order to form GaAs crystal structure (zincblende).

[44] In both defect cases the center of mass (CM) of the nitrogen dimer is shifted slightly away from the CM of the tetrahedron (inside which the dimer is located) as measured along the [111] direction, toward the base of the tetrahedron. These shifts in the I_{NN}^{tGa} and I_{NN}^{tAs} interstitial cases are 0.18 and 0.33 Å, respectively.

[45] K. Laaksonen, H.-P. Komsa, E. Arola, T. T. Rantala, and R. M. Nieminen (unpublished).

[46] The theoretical study of substitutionally random $GaAs_{1-x}N_x$ alloys by Bellaiche, Wei, and Zunger (Ref. 8) throughout the whole composition range shows that the bandgap decreases monotonically, when x increases from $x=0$ to $x \sim 0.5$ (see Fig. 4 of Ref. 8).

[47] Considering the accuracy of the calculated changes in the electronic band structure of GaAs due to I_{N}^{eGa}-type interstitials, it should be noticed that the changes of energies of the extended states, coupled to these interstitials, depend on the volume of the supercell used. In our case, both the single N atom and NN dimer interstitials in GaAs calculations are based on using a 64-atom unit cell.

[48] We will later on study the changes in the electronic structure of $GaAs_{1-x}N_x$ alloys when a substitutional nitrogen defect transforms into an interstitial one, within the framework of the density functional theory (DFT). This hopefully sheds some more light onto the blue- and redshift arguments of Loke *et al.* (Ref. 25).